Line-shape comparison of electromagnetically induced transparency and Raman Ramsey fringes in sodium vapor

Ichiro Yoshida, Nobuhito Hayashi, Kazuki Fujita, Shuya Taniguchi, Yoshitaka Hoshina, and Masaharu Mitsunaga*
Graduate School of Science and Technology, Kumamoto University, 2-39-1 Kurokami, Kumamoto, 860-8555, Japan
(Received 26 December 2012; published 22 February 2013)

We have simultaneously studied electromagnetically induced transparency (EIT) and Raman Ramsey fringes (RRF) in sodium vapor, in the same theoretical framework and the same experimental scheme. RRF spectra and EIT spectra can be simply distinguished by whether the gate timing of the detection is set at the beginning (RRF) or at the end (EIT) of the excitation pulses. The EIT spectral peaks exhibited pronounced ac Stark shifts linearly depending upon the pumping power (8.8 kHz/mW), while in the RRF spectra such shifts were almost negligible (0.19 kHz/mW), provided that the pulse separation is sufficiently large. This fact promotes RRF as a strong candidate for next-generation compact atomic clocks. Transient spectra in between RRF and EIT have also been investigated by changing the gate timing within the excitation pulse, and the transition time from RRF to EIT was found to be of the order of a few microseconds.

DOI: 10.1103/PhysRevA.87.023836 PACS number(s): 42.65.Dr, 42.50.Gy

I. INTRODUCTION

Development of simple, compact-size, and high-accuracy atomic clocks has long been needed for many applications such as GPS (global positioning system) receivers, underwater sensor systems, and so on. Electromagnetically induced transparency (EIT) [or, coherent population trapping (CPT)] [1–3] has been one of the strong candidates for such applications [4–7]. In EIT, two waves called probe (frequency ω_p) and coupling (ω_c) are applied to an atomic vapor having a three-level Λ system [see Fig. 1(a)], and the EIT signal is observed as an increase in the transmission spectrum when the two-photon resonance condition ($\omega_p - \omega_c = \omega_{21}$) is satisfied, where ω_{21} denotes the sublevel splitting frequency of the atom. Since an EIT-based atomic clock does not need a microwave cavity compared to an optical-RF double-resonance-type clock, it reduces the device size considerably. One severe drawback of an EIT clock, however, may be the ac Stark shift, where the signal peak shifts linearly with the pumping laser power. This effect obviously leads to erroneous operation of the atomic clocks. On the other hand, in the case of recently investigated Raman Ramsey fringes (RRFs) [8–10] (Ramsey fringes due to stimulated Raman resonances [11,12]), where probe and coupling beams are applied in a pulsed manner, such peak shifts are reported to be much smaller, or almost negligible. Although experimental results of RRF have already been reported in several papers [13–15], a theoretical approach as well as detailed comparison of theory and experiment for RRF and EIT have been left uninvestigated. Considering this situation, it is now very important to present a unified theory for EIT and RRF in order to perform systematic measurement, and to compare these two as possible candidates for the next-generation atomic clocks.

The purpose of this paper is to theoretically and experimentally investigate EIT and RRF phenomena simultaneously by using a hot sodium vapor, and compare the two line shapes. We find that both EIT and RRF can be studied in one theoretical framework, or in a single experimental setup. Figure 1(b) shows the pulse timing sequences in our experiment. Both probe and coupling beams are pulsed with pulse duration τ and separation T. (In this paper, we employ names "probe" and "coupling" to be consistent with our previous papers, but probe is not necessarily weak compared to coupling. On the contrary, through this paper probe and coupling powers are equal.) The pulse duration τ is assumed to be much longer than any decay times. Now the transmitted powers are monitored with a gated (boxcar) integrator. When the gate timing is set at the end of the pulse, we are to observe an EIT spectrum, because the system is safely in a two-mode, three-level steady state. On the other hand, when the gate is set at the beginning of the pulse, we will observe an RRF spectrum because the transmission is modified due to the free precession of the sublevel coherence. In this way, only by the gate timing, both EIT and RRF spectra can be obtained. Besides, by varying the gate timing t from $t = 0$ (beginning of the pulse) to $t = \tau$, the transient behavior from RRF spectra to EIT spectra should be studied, as will be shown later.

What we found in our theoretical and experimental study was that the peaks of the EIT spectra are severely shifted to the high-frequency side due to the ac Stark shift. On the other hand, the peaks of the RRF central fringes are almost exactly at the true clock transition, provided that the pulse separation T is sufficiently large. Consequently, RRF is much superior to EIT for the atomic clock application. In the following sections we first present our theoretical analysis in this EIT-RRF system. Our experimental setup will then be briefly mentioned and the detailed experimental results will be finally given.

II. THEORY

The purpose of this theory section is to analytically derive the line shapes for EIT and RRF in a unified manner and to investigate the transient behavior from RRF to EIT when the gate timing is varied from $t = 0$. Also, we will study the transition from EIT to RRF when the pulse separation T is increased from 0. In particular, we are interested in the dependence of the line shapes on the probe power I_p and the coupling power I_c, both of which can become strong so that

*mitunaga@sci.kumamoto-u.ac.jp

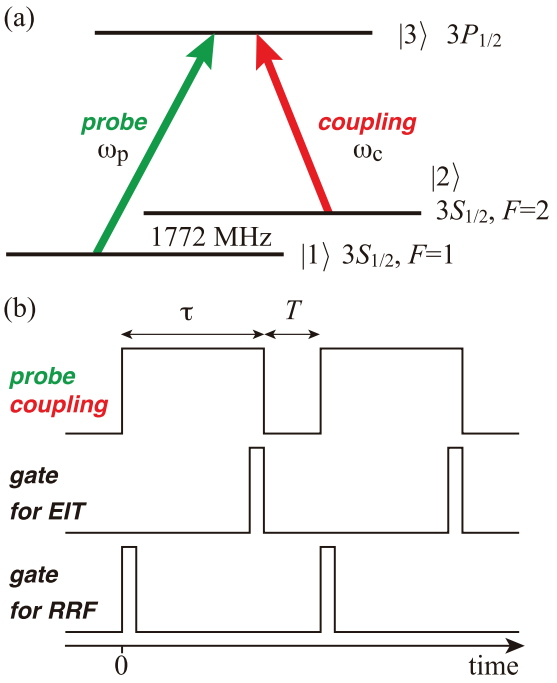

FIG. 1. (Color online) (a) Related energy-level scheme for EIT and RRF in sodium vapor. (b) Pulse sequence for EIT and RRF experiments.

they will be treated nonperturbatively. In order to extract only the intrinsic features of the phenomenon, we will simplify the problem as much as possible.

As for the atomic system, we assume a three-level system as shown in Fig. 1(a). In the real situation, the level $|1\rangle$ corresponds to $3S_{1/2}$, $F=1$, $|2\rangle$ to $3S_{1/2}$, $F=2$, and $|3\rangle$ to $3P_{1/2}$, $F'=1$ or $F'=2$ level of the sodium atom, respectively. The pulse sequence is given in Fig. 1(b). Now we investigate the time evolution of the sublevel coherence, the optical coherences, and the absorption coefficient.

The Liouville equations for the optical coherences ρ_{13} and ρ_{23}, and the ground-state sublevel coherence ρ_{12}, can be written as [16]

$$\dot{\rho}_{13} = (i\omega_{31}-\gamma)\rho_{13} - \frac{i}{2}\sum_j \Omega_j^* e^{i\omega_j t} n_{13} - \frac{i}{2}\sum_j \Omega_j^* e^{i\omega_j t}\rho_{12}$$

$$\dot{\rho}_{23} = (i\omega_{32}-\gamma)\rho_{23} - \frac{i}{2}\sum_j \Omega_j^* e^{i\omega_j t} n_{23} - \frac{i}{2}\sum_j \Omega_j^* e^{i\omega_j t}\rho_{21}$$

$$\dot{\rho}_{12} = (i\omega_{21}-\gamma_s)\rho_{12} + \frac{i}{2}\sum_j \Omega_j^* e^{i\omega_j t}\rho_{32} - \frac{i}{2}\sum_j \Omega_j e^{-i\omega_j t}\rho_{13}, \quad (1)$$

where ω_{ij} is the level splitting frequency and $n_{\ell 3} = n_\ell - n_3$ is the population difference between level ℓ ($\ell = 1$ or 2) and level 3, and $\Omega_j = 2p\mathcal{E}_j/\hbar$ is the Rabi frequency ($j = p,c$) for probe and coupling, assuming, for simplicity, that the two transitions 1-to-3 and 2-to-3 have the same dipole moment p. γ and γ_s are the optical and sublevel dephasing rates, respectively. In ordinary textbook-style derivation of EIT, nonresonant contributions are neglected so that the probe interacts only on the 1-to-3 transition and coupling only on the 2-to-3 transition. Here we are interested in derivation of the ac Stark shift in EIT, and so we will keep nonresonant contributions in the above equations.

These equations can be solved by Fourier decomposing the optical coherences $\rho_{\ell 3}$ as

$$\rho_{\ell 3}(t) = \rho_{\ell 3s}e^{i\omega_s t} + \rho_{\ell 3c}e^{i\omega_c t} + \rho_{\ell 3p}e^{i\omega_p t} + \rho_{\ell 3a}e^{i\omega_a t}, \quad (2)$$

where the coherences are assumed to have Stokes ($\omega_s = \omega_c - \omega_0$) and anti-Stokes ($\omega_a = \omega_p + \omega_0$) components [17,18]. On the other hand, the sublevel coherence ρ_{12} has only a ω_0 component and can be expressed as

$$\rho_{12}(t) = \rho_{12u}(t)e^{i\omega_0 t}. \quad (3)$$

Here we apply the adiabatic following approximation [19], which states that the optical coherence decay γ is so rapid compared to the sublevel coherence decay γ_s that all the optical coherence coefficients $\rho_{\ell 3 j}$ appearing in Eq. (2) will adiabatically follow the motions of ρ_{12u}, n_{13}, and n_{23} and thus can be solved as steady-state solutions. By substituting these results for the sublevel coherence component ρ_{12u}, the equation of motion for ρ_{12u} is given by

$$\dot{\rho}_{12u} = -\gamma_s'\rho_{12u} - A. \quad (4)$$

Here the coefficients γ_s' and A are defined by

$$\gamma_s' \equiv \gamma_s + i\delta_s + \frac{1}{4}\frac{|\Omega_c|^2}{\gamma_{s32}} + \frac{1}{4}\frac{|\Omega_c|^2}{\gamma_{p31}^*} + \frac{1}{4}\frac{|\Omega_p|^2}{\gamma_{c32}} + \frac{1}{4}\frac{|\Omega_p|^2}{\gamma_{a31}^*} \quad (5)$$

and

$$A \equiv \frac{1}{4}\left(\frac{n_{23}}{\gamma_{c32}} + \frac{n_{13}}{\gamma_{p31}^*}\right)\Omega_p^*\Omega_c, \quad (6)$$

where the two-photon detuning $\delta_s \equiv \omega_0 - \omega_{21}$, and $\gamma_{j3\ell} \equiv \gamma - i(\omega_j - \omega_{3\ell})$ ($j = s,c,p,a; \ell = 1,2$). This equation of motion for ρ_{12u} [Eq. (4)] should be solved in three different ways. First, in the EIT limit, where the pulse separation T is long enough that everything is in a steady state, ρ_{12u}^{EIT} for the EIT case is simply given by

$$\rho_{12u}^{EIT} = -\frac{A}{\gamma_s'}, \quad (7)$$

and this represents the EIT line shape. Although this line shape is very complicated, it can be reduced to a simple Lorentzian if we make some assumptions. In the expression of Eq. (5), if we assume that $\omega_{21} \gg \gamma$, $\omega_p \approx \omega_{31}$, and $\omega_c \approx \omega_{32}$, then $\gamma_{s32} \approx i\omega_{21}$, $\gamma_{p31}^* \approx \gamma$, $\gamma_{c32} \approx \gamma$, and $\gamma_{a31}^* \approx i\omega_{21}$, and γ_s' can be rewritten as

$$\gamma_s' \approx \gamma_s + \frac{|\Omega_{total}|^2}{4\gamma} + i\left[\delta_s - \frac{|\Omega_{total}|^2}{4\omega_{21}}\right]. \quad (8)$$

where $|\Omega_{total}|^2 = |\Omega_c|^2 + |\Omega_p|^2$. We notice that in this case Eq. (7) is a simple Lorentzian with a peak $\delta_s = |\Omega_{total}|^2/4\omega_{21}$ ac Stark shifted, and a width $\gamma_s + |\Omega_{total}|^2/4\gamma$ saturation broadened. It should be emphasized that both the peak shifts and the linewidths of EIT linearly depend on the total power of probe and coupling.

In the second way of solving Eq. (4), we consider the free-precession period, where both the excitation pulses are off. Here, by substituting $\Omega_c = \Omega_p = 0$ into Eq. (4), we obtain the simple form as

$$\dot{\rho}_{12u} = -(\gamma_s + i\delta_s)\rho_{12u}. \tag{9}$$

In this way the ρ_{12u}^{RRF} for RRF is simply related to ρ_{12u}^{EIT} as

$$\rho_{12u}^{RRF} = \rho_{12u}^{EIT} e^{-(\gamma_s + i\delta_s)T}. \tag{10}$$

The third way of solving Eq. (4) is to obtain a general solution. Here γ_s' is always a constant of motion. In the expression of A, n_{13} and n_{23} may depend on t. However, when $n_{13} + n_{23}$ is constant in time, A can be treated as constant also. In this case, the solution of Eq. (4) is straightforward and given by

$$\rho_{12u}(t) = \rho_{12u}^{EIT}(1 - e^{-\gamma_s' t}) + \rho_{12u}^{RRF} e^{-\gamma_s' t}. \tag{11}$$

Remember that experimentally t represents the gate timing and when the gate is at the beginning of the pulse ($t = 0$), it gives the RRF line shape [$\rho_{12u}(0) = \rho_{12u}^{RRF}$], and when the gate is at the end of the pulse ($t = \infty$), it goes back to the EIT line shape [$\rho_{12u}(\infty) = \rho_{12u}^{EIT}$]. Once the sublevel coherence ρ_{12u} is obtained, the optical coherences ρ_{13} and ρ_{23}, and subsequently the absorption coefficients α_p (α_c) for the probe (coupling) pulse, can be obtained immediately by assuming the adiabatic following approximation. They are given by

$$\alpha_p(t) = \alpha_0\gamma\left[\frac{n_{13}}{\gamma_{p31}} + \frac{n_{23}}{\gamma_{p32}} + \frac{1}{\gamma_{p31}}\frac{\Omega_c}{\Omega_p}\rho_{12u}^*(t)\right] \tag{12}$$

and

$$\alpha_c(t) = \alpha_0\gamma\left[\frac{n_{13}}{\gamma_{c31}} + \frac{n_{23}}{\gamma_{c32}} + \frac{1}{\gamma_{c32}}\frac{\Omega_p}{\Omega_c}\rho_{12u}(t)\right], \tag{13}$$

where $\alpha_0 = kNp^2/\epsilon_0\hbar\gamma$ is the peak linear absorption coefficient with atomic density N. Exactly speaking, n_{13} and n_{23} are dependent on time because they decrease and increase when the excitation pulses are turned on and off, respectively. Such variation can be neglected when the pumping rates $P_{13} = |\Omega_p|^2/2\gamma$ for the 1-to-3 transition and $P_{23} = |\Omega_c|^2/2\gamma$ for the 2-to-3 transition are small compared to the spontaneous emission rate Γ.

The real part of $-\alpha_p(t)$ in the above expression directly represents the experimentally observed transmission spectra and is numerically simulated in Fig. 2, which is a contour plot of $-\mathrm{Re}[\alpha_p]$ as functions of probe detuning δ_p and gate timing t. The parameters used in this simulation were $T = 8\ \mu$s, $\Omega_p/2\pi = \Omega_c/2\pi = 10$ MHz, and $\delta_c = 0$ MHz. As for the optical dephasing rate γ, $\gamma/2\pi$ would be a half of the natural linewidth (10 MHz) without a buffer gas, but with a buffer gas, γ increases considerably. It is rather difficult to measure γ but we set $\gamma/2\pi = 500$ MHz to fit the data. The sublevel dephasing rate γ_s, on the other hand, is given by the inverse of the time an atom stays within the optical beam. This can be measured by the RRF decay time as a function of the pulse separation T [see Eq. (10). and also see Fig. 4], and we set it as $\gamma_s/2\pi = 0.03$ MHz. In Fig. 2, when the gate time $t = 0$, the fringe pattern is clearly observed indicating the RRF spectrum. As t becomes large, the fringes gradually disappear and only one peak becomes pronounced, indicating the EIT

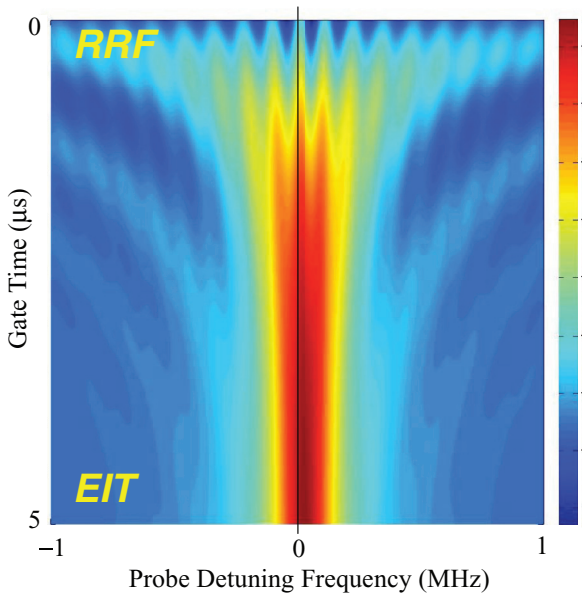

FIG. 2. (Color online) Contour plot of transmitted probe power, or $-\mathrm{Re}[\alpha_p]$, vs probe detuning frequency for various gate times t. The spectra at $t = 0$ and $t = 5\ \mu$s represent RRF and EIT, respectively.

spectrum. Note that the EIT peak is slightly shifted from the clock transition to the right by the ac Stark shift. Exactly the same plot should be obtained for α_c, since the expression for α_p and α_c are symmetrical and become the same when $\Omega_p = \Omega_c$.

It should also be noted that Eq. (12) can become an ordinary textbook EIT expression α^{EIT} [20,21]

$$\alpha^{EIT} = \frac{\alpha_0\gamma}{\gamma - i(\omega_p - \omega_{31}) + \frac{|\Omega_c|^2/4}{\gamma_s - i\delta_s}}, \tag{14}$$

for the absorption coefficient when we assume that $n_{13} = 1$, $n_{23} = 0$, $|\Omega_p|^2$ is negligible, and the γ_{s32} term is negligible. However, this expression cannot explain the ac Stark shift of the EIT signal peak. The ac Stark shift appears only when we take the Stokes or anti-Stokes coherences into the theory.

In this whole theory section we have neglected the inhomogeneous broadening due to the Doppler distribution. The extension of this theory, however, to the inhomogeneous case is straightforward. In fact, we have calculated the RRF line shapes for various Doppler shifts $\delta_s = kv$, where v is the atomic velocity. The line shapes hardly changed with various δ_s values, and we can safely say that inclusion of the Doppler broadening will not change our results.

III. EXPERIMENT

The experimental setup was similar to our previous EIT studies in Na vapor [16,22,23], as illustrated in Fig. 3. The light source was a single-frequency tunable ring dye laser (Coherent CR699-21) tuned to the $3S_{1/2} - 3P_{1/2}$ D_1 transition [24] of the Na atom at 589.6 nm. First, by using the acousto-optic modulator $(\mathrm{AOM})_1$, the output beam was pulsed on and off with repetition time 250 μs. The pulse separation T can be varied from 0 to several tens of microseconds. The beam was then divided for coupling and probe as shown in Fig. 3. The coupling beam had a fixed frequency shift of −200 MHz with

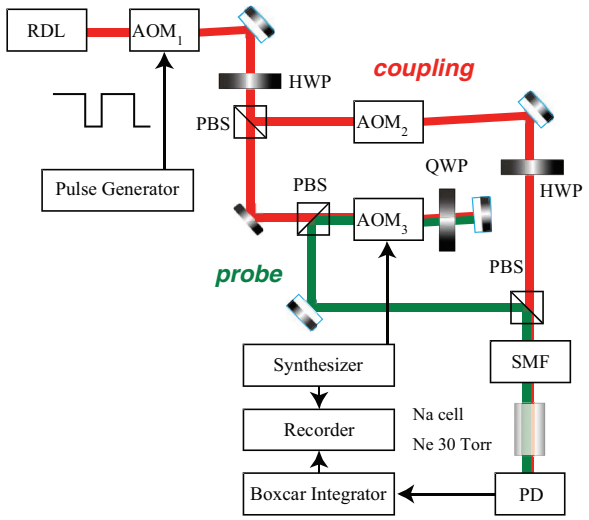

FIG. 3. (Color online) Schematic of the experimental setup: RDL, ring dye laser; AOM, acousto-optic modulator; PBS, polarizing beam splitter; HWP, half-wave plate; QWP, quarter-wave plate; PD, photodetector.

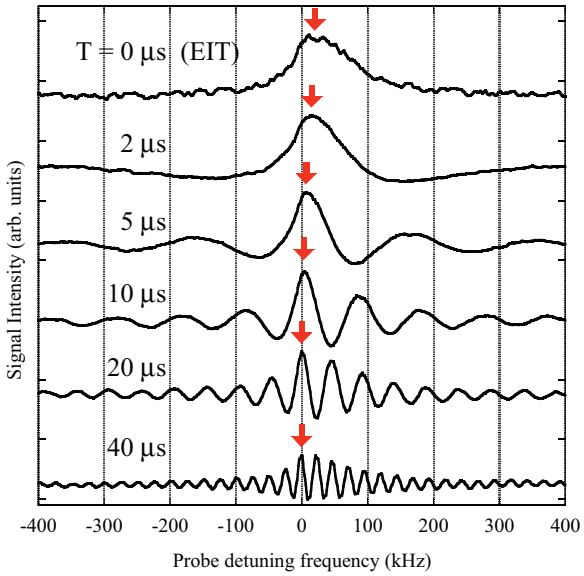

FIG. 4. (Color online) Probe transmission spectra for various pulse separation T. The curve for $T = 0$ represents the EIT spectrum. Red arrows indicate the peak positions.

AOM_2, while the probe beam was variably frequency shifted by $+1571.6 \pm 1$ MHz by using an rf synthesizer in a double-pass configuration with AOM_3. In this way, the resultant probe-coupling frequency difference can be varied around the Na hyperfine splitting frequency 1771.626 MHz. The two beams, after passing a single-mode fiber to improve the transverse mode quality, collinearly impinged on a glass cell containing a hot sodium atomic vapor with a Ne buffer gas of 30 Torr. Both the beam spot sizes FWHM were 400 μm. A longitudinal magnetic field of 2.1 G inside a magnetic shielding was applied to extract only the field-insensitive transition [25]. Both the probe powers I_p and the coupling powers I_c were made equal in every experiment, so that the important parameter is the total laser power $I_t = I_p + I_c$. The transmitted probe and coupling powers were detected by a photodetector and analyzed by a gated integrator whose gate width was typically 60 ns, which was much shorter than the pulse width τ and the gate timing t could be varied arbitrarily. For RRF measurement, the gate t is set at the beginning of the pulse ($t = 0$), while for EIT t was set at the end of the pulse ($t = \tau$). All the data were taken by scanning the frequency synthesizer while monitoring the gated integrator output.

IV. RESULTS

As the first measurement, the pulse separation T is varied from $T = 0$ μs (continuous excitation) to 2, 5, 10, 20, and 40 μs with the gate pulse fixed at RRF position. Figure 4 shows the results. First of all, when $T = 0$ a single EIT peak is observed but, as anticipated, the peak is ac Stark shifted towards the higher frequency side compared to the clock frequency (probe detuning $\delta_s = 0$). When T is gradually increased, the number of fringes increases accordingly and the fringe spacing is indeed given by T^{-1}. Also, the central fringe peak positions indicated by the red arrows approach the clock frequency and finally it is "locked" to $\delta_s = 0$. These findings already claim that RRF peaks exhibit more precise clock frequency for sufficiently large T.

One of our main concerns is how the excitation laser powers affect the EIT-RRF line shapes, especially peak positions and the linewidths. Figure 5 shows our main results of EIT-RRF line shapes for various total laser powers I_t. Here the EIT line shapes and RRF line shapes exhibit clearly different behaviors of power dependence. In the EIT case, the peak positions (indicated by red arrows) shift towards the right linearly with I_t, and also the saturation broadening (also proportional to I_t) is clearly seen. On the other hand, for RRF, the central fringe peak position hardly moves from the clock frequency and the signal linewidth (defined by a half of the central fringe separation) is almost the same. This strongly supports that RRF is much more robust against power fluctuation. The EIT and RRF line-shape asymmetry observed in Fig. 5 (for example, the 6.0-mW case, which has a rather sharp rise in the left wing and a slow fall in the right wing) may be explained by assuming the Gaussian transverse mode profile of the probe and coupling beams. In this case the Rabi frequencies are not uniquely determined but are distributed within some range. Then the superposition of narrow unshifted line shapes and broad ac-Stark-shifted line shapes will result in such asymmetric shapes as shown in Fig. 5.

More detailed and quantitative analyses are given in Figs. 6 and 7. Figure 6 is the plot of peak positions vs total beam power I_t for EIT and RRF, and both the slopes are well approximated by linear lines. The fitted slopes gave 8.8 kHz/mW for EIT and 0.19 kHz/mW for RRF. [In terms of power density, they are expressed as 64 Hz/(mW/cm^2) for EIT and 1.4 Hz/(mW/cm^2) for RRF.] This shows a 46 times improvement of the peak shift of the clock transition by using the RRF method. Figure 7 shows the linewidths vs I_t for EIT and RRF. Once again, both slopes are linear functions of I_t and the fitted slopes gave 32 kHz/mW for EIT and 0.48 kHz/mW for RRF. This time the enhancement factor is 67. Remember that the RRF linewidths

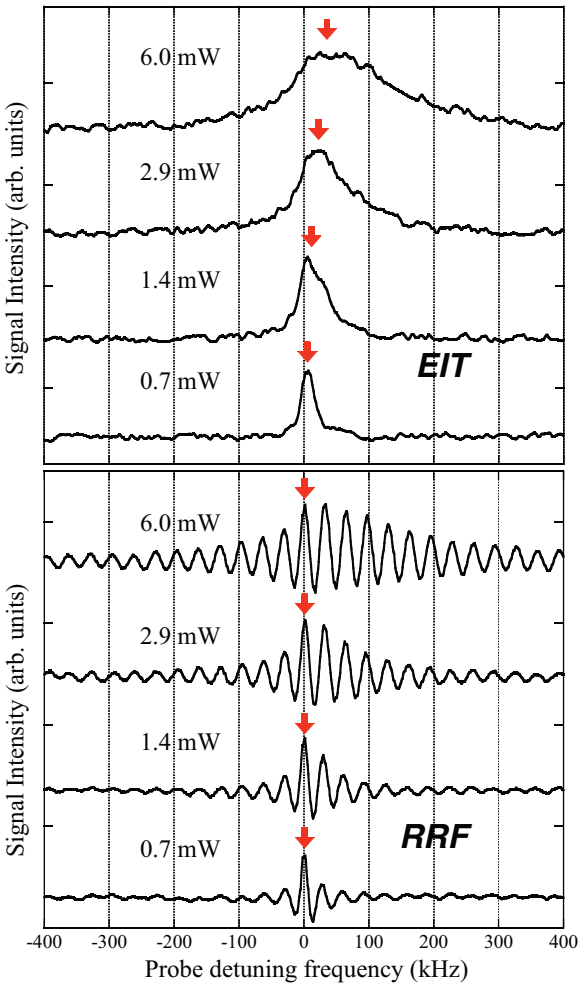

FIG. 5. (Color online) EIT spectra (upper figure) and RRF spectra (lower figure) for various total beam power $I_t = 6.0$, 2.9, 1.4, and 0.7 mW. Red arrows indicate the peak positions.

can be narrowed by increasing the pulse separation T but with a sacrifice of the reduction in signal intensity.

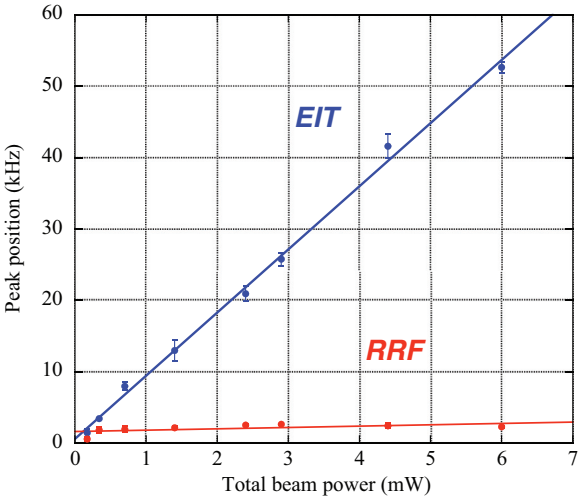

FIG. 6. (Color online) Signal peak position vs total beam power for EIT and RRF.

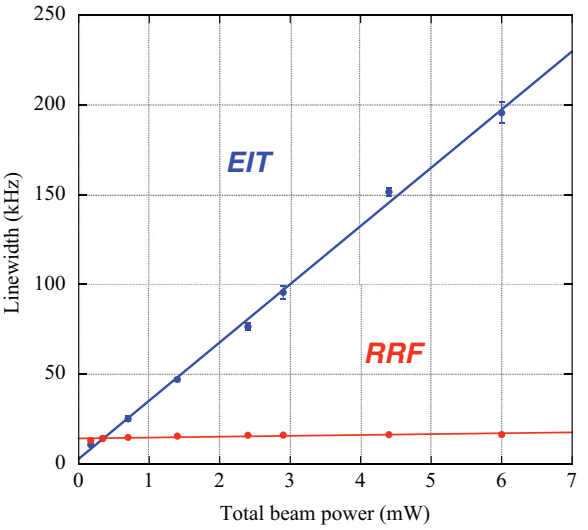

FIG. 7. (Color online) Linewidth vs total beam power for EIT and RRF.

Finally the transient behavior from RRF line shapes to EIT line shapes has been investigated, as shown in Fig. 8. This measurement may be important because we need to know the characteristic time scale of the fringe decay. (Theoretically this is expressed in Fig. 2.) By changing the gate pulse timing from $t = 0$ to several tens of microseconds, it is clearly seen that the RRF line shape gradually returns to the EIT line shape, losing the fringe information, and the signal peak moves back to the original ac-Stark-shifted peak. The characteristic fringe decay time is of the order of a few microseconds, and the decay time is given by the inverse of the saturation broadened EIT linewidth, as expected from the theory section. Of course, in order to obtain a nice RRF line shape, the gate width has to be of the order of this decay time.

V. CONCLUSION

We have simultaneously studied EIT and RRF in a two-mode, three-level system by using a hot sodium vapor, both

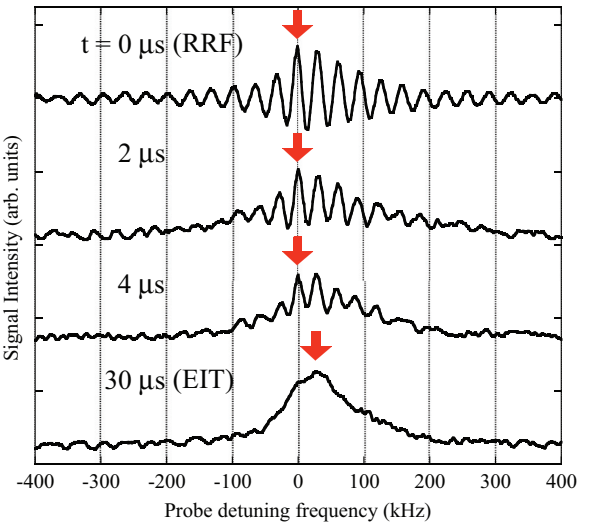

FIG. 8. (Color online) Transition from RRF to EIT by varying the gate timing t. From top to bottom, $t = 0$, 2, 4, and 30 μs.

theoretically and experimentally. The transmission spectra were found to switch between RRF and EIT, depending upon whether the beginning or the end of the pulse is gated for detection. Besides, by changing the gate position gradual transition from RRF to EIT could be observed, in agreement with the theoretical prediction.

Comparisons of EIT and RRF line shapes were extensively studied both theoretically and experimentally, especially from the viewpoint of application to next-generation compact-size atomic clocks. We have found that, both in terms of signal peak position stability and linewidth stability, RRF is far superior to EIT, due to pronounced ac Stark shifts for EIT. This fact should promote RRF as a strong candidate for next-generation compact atomic clocks. Although this work has been performed in a sodium vapor, a similar theoretical and experimental study should be possible in other alkali metals such as rubidium and cesium.

Finally, we should point out that such an RRF type of very high-resolution spectroscopy can be applied for monitoring very small pulsed perturbations taking place in the free-precession period. For example, a pulsed perturbation such as ac Stark shift with magnitude 10 kHz and duration 10 μs should cause a 0.1π radian phase shift of the RRF fringes, which is easily detectable. The challenge of monitoring this type of phase shift is underway in our laboratory.

[1] R. G. Brewer and E. L. Hahn, Phys. Rev. A **11**, 1641 (1975).

[2] K.-J. Boller, A. Imamoğlu, and S. E. Harris, Phys. Rev. Lett. **66**, 2593 (1991).

[3] J. E. Field, K. H. Hahn, and S. E. Harris, Phys. Rev. Lett. **67**, 3062 (1991).

[4] S. Brandt, A. Nagel, R. Wynands, and D. Meschede, Phys. Rev. A **56**, R1063 (1997).

[5] R. Wynands, A. Nagel, S. Brandt, D. Meschede, and A. Weis, Phys. Rev. A **58**, 196 (1998).

[6] R. Wynands and A. Nagel, Appl. Phys. B **68**, 1 (1999).

[7] M. Merimaa, T. Lindvall, I. Tittonen, and E. Ikonen, J. Opt. Soc. Am. B **20**, 273 (2003).

[8] J. E. Thomas, P. R. Hemmer, S. Ezekiel, C. C. Leiby, Jr., R. H. Picard, and C. R. Willis, Phys. Rev. Lett. **48**, 867 (1982).

[9] T. Zanon, S. Guerandel, E. de Clercq, D. Holleville, N. Dimarcq, and A. Clairon, Phys. Rev. Lett. **94**, 193002 (2005).

[10] S. G. Pati, K. Salit, R. Tripathi, and M. S. Shahriar, Opt. Commun. **281**, 4676 (2008).

[11] P. R. Hemmer, G. P. Ontai, and S. Ezekiel, J. Opt. Soc. Am. B **3**, 219 (1989).

[12] P. R. Hemmer, M. S. Shahriar, V. D. Natoli, and S. Ezekiel, J. Opt. Soc. Am. B **6**, 1519 (1989).

[13] S. Guérandel, T. Zanon, N. Castagna, F. Dahes, E. de Clercq, N. Dimarcq, and A. Clairon, IEEE Trans. Instrum. Meas. **56**, 383 (2007).

[14] N. Castagna, R. Boudot, S. Guérandel, E. de Clercq, N. Dimarcq, and A. Clairon, IEEE Trans. Ultrason. Ferroelectr. Freq. Control **53**, 246 (2009).

[15] Y. Yano and S. Goka, Jpn. J. Appl. Phys. **51**, 122401 (2012).

[16] K. Takahashi, N. Hayashi, H. Kido, S. Sugimura, N. Hombo, and M. Mitsunaga, Phys. Rev. A **83**, 063824 (2011).

[17] K. Harada, T. Kanbashi, M. Mitsunaga, and K. Motomura, Phys. Rev. A **73**, 013807 (2006).

[18] K. Harada, K. Mori, J. Okuma, N. Hayashi, and M. Mitsunaga, Phys. Rev. A **78**, 013809 (2008).

[19] S. M. Shahriar, P. R. Hemmer, D. P. Katz, A. Lee, and M. G. Prentiss, Phys. Rev. A **55**, 2272 (1997).

[20] M. O. Scully and M. S. Zubairy, *Quantum Optics* (Cambridge University Press, Cambridge, UK, 1997).

[21] P. Meystre and M. Sargent III, *Elements of Quantum Optics* (Springer, Berlin, 2007); *Nonlinear Optics* (Academic Press, New York, 1997).

[22] N. Hayashi, A. Fujisawa, H. Kido, K. Takahashi, and M. Mitsunaga, J. Opt. Soc. Am. B **27**, 1645 (2010).

[23] N. Hombo, S. Taniguchi, S. Sugimura, K. Fujita, and M. Mitsunaga, J. Opt. Soc. Am. B **29**, 1717 (2012).

[24] M. Stähler, R. Wynands, S. Knappe, J. Kitching, L. Hollberg, A. Taichenachev, and V. Yudin, Opt. Lett. **27**, 1472 (2002).

[25] Y. Y. Jau, E. Miron, A. B. Post, N. N. Kuzma, and W. Happer, Phys. Rev. Lett. **93**, 160802 (2004).